

Study of Influencing Factors on Charge Exchange Efficiency from C^{2+} to C^{-} Using Geant4

Authors: Li, Wangxuan, Liu, Dr. Huan-Ling, Dr. Shengli Wang, Li, Prof. Deming, Wang, Ms. Junyan, Liu, Dr. Huan-Ling

Date: 2025-07-04T16:25:01+00:00

Abstract

A first attempt to simulate the charge exchange process from C^{2+} to C^{-} using the Monte Carlo software Geant4 has been accomplished, modeling low-energy C^{2+} ions passing through an exchange medium. The yields of C^q ($q=-2, -1, 0, \text{ and } +1$) from injected C^{2+} with different energies into different exchange media are measured by setting up the physical model in the simulation program. The effect of different energies (ranging from 60 to 300 keV), different exchange media (isobutene and methane), and different density distributions of exchange medium in the charge exchange cell on the charge exchange efficiency have been studied. The comparison of the present results with experimental results shows the feasibility of this method. Moreover, the present results demonstrate that low-density diffuse regions on either side of the high-density central region in the charge exchange cell have a significant contribution to improving the charge exchange efficiency. The charge exchange efficiency in organic non-metallic gases of isobutene is higher than in methane; particularly, an efficiency close to 2% of C^{2+} to C^{-} conversion can be achieved in methane.

Full Text

Preamble

A First Attempt to Simulate the Charge Exchange Process from C^{2+} to C^{-} Using Geant4

Wang-Xuan Li,^{1,2} Huan-Ling Liu,^{1,†} Sheng-Li Wang,^{1,‡} De-Ming Li,¹ and Jun-Yan Wang^{1,2}

¹Shanghai Institute of Applied Physics, Chinese Academy of Sciences, Shanghai 201800, China

²University of Chinese Academy of Sciences, Beijing 100049, China

We have accomplished a first attempt to simulate the charge exchange process of C^{2+} to C^- , in which low-energy C^{2+} ions pass through an exchange medium, using the Monte Carlo software Geant4. The yields of C^q ($q = -2, -1, 0,$ and $+1$) from injected C^{2+} ions with different energies into different exchange media are measured by establishing a physical model in the simulation program. The effects of different energies (ranging from 60 to 300 keV), different exchange media (isobutene and methane), and different density distributions of the exchange medium in the charge exchange cell on the charge exchange efficiency have been studied. Comparison of our results with experimental data demonstrates the feasibility of this method. Moreover, our results demonstrate that low-density diffuse regions on either side of the high-density central region in the charge exchange cell make a significant contribution to improving the charge exchange efficiency. The charge exchange efficiency in the organic non-metallic close to 2% for C^{2+} to C^- can be achieved in methane.

Keywords: Charge exchange, Ion yields, Charge exchange efficiency, Monte Carlo simulation, Geant4

INTRODUCTION

Radiocarbon (^{14}C), as one of the long-lived radioactive isotopes, has been scientifically applied in various fields such as archaeology, astrophysics, earth and environmental sciences, and biomedical research [1–7]. Accurate measurement of ^{14}C has attracted considerable attention from scientists. Accelerator mass spectrometry (AMS), currently the most powerful technique for measuring ^{14}C , has evolved through versatile, specialized equipment, and miniaturization stages since the late 1970s, achieving high accuracy with isotopic abundances as low as 10^{-16} [6, 8–13]. Moreover, AMS has been evolving toward lower ion energies, more compact designs, and greater cost-effectiveness to accommodate increasing diverse demands [14–16].

One major difficulty in measuring ^{14}C using AMS is eliminating interfering isobars such as ^{14}N and molecules like $^{12}CH_2$ and ^{13}CH [17, 18]. Conventional AMS systems, which employ a negative ion source (since $^{14}N^-$ ions are not stable) and charge-stripping devices to convert $^{14}C^-$ to multiply-charged positive ions ($^{14}C^{n+}$, $n \geq 1$), typically require high ion energies to ensure accurate measurements because molecular ions have no bound states. Many related studies have been published, and today's smallest available conventional AMS systems operate with ion energies below 150 keV [17, 19–24]. In addition, with significant development of Electron Cyclotron Resonance (ECR) ion sources in recent decades, a new type of low-energy AMS (<100 keV) has rapidly emerged, such as the PIMS system jointly developed by NEC and SUERC [25, 26] and PKU-PIMS developed by Peking University [27]. These systems attempt to utilize the inverse process of conventional AMS, which was proposed by Roy Middleton at the first international accelerator mass spectrometry conference in 1978 [28].

The main principle of this type of AMS, which we call positive-ion AMS, is as follows: by extracting C^{n+} ions from an ECR ion source to eliminate interference from molecular ions and passing them through a charge exchange cell (CEC) to generate C^- ions, interference from N^- ions can be eliminated. To date, ECR ion sources can obtain C^{n+} beam currents ranging from several microamperes to several hundred microamperes using carbon-containing gas samples [12, 29]; however, the charge exchange efficiency in CEC remains low and the underlying mechanism remains unclear [25, 27].

The process of converting C^{n+} to C^- in a CEC is very complicated, involving interactions between C^{n+} ions and a medium that lead to electron capture and formation of C^- ions. Based on real AMS devices, Prof. Freeman and colleagues [25] proposed that for different target materials, as the energy of incident C^{2+} ions increases, the yield of C^- ions gradually decreases, and the energy of C^{2+} ions required for charge exchange should not be too high. In 2015, K. Li and colleagues [27] found during experiments with C^{2+} ions passing through a mixture of ethylene and Ar gas that as gas concentration increases, the difference in C^- ion production gradually increases. At a gas flow rate of 5 SCCM, the conversion efficiency from C^{2+} to C^- can reach 5%.

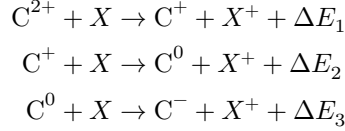
In this study, Monte Carlo methods are employed to directly calculate the charge state distribution of C^{2+} ions interacting with different media. By adjusting the geometric distribution of different media, we explore the fundamental principles influencing charge exchange efficiency, aiming to provide theoretical insights for the charge exchange process in practical devices.

II. THE MECHANISM OF CHARGE EXCHANGE

The central role of the charge exchange cell in a positive-ion AMS device is to realize the charge exchange process of charged ions. In general, when an ion with an initial charge state q , nuclear charge number Z , and initial energy E_0 passes through an exchange medium (target material) with thickness x , the relationship between the charge state distribution and the charge exchange cross-section can be described by the following linear coupled differential equation [30]:

$$\frac{d\Phi_q(E_0, x)}{dx} = \sum_{q' \neq q} \Phi_{q'}(E_0, x) \sigma_{q', q}(E_0, Z) - \Phi_q(E_0, x) \sum_{q' \neq q} \sigma_{q, q'}(E_0, Z)$$

where Φ_q and $\Phi_{q'}$ are the transient proportions in charge states q and q' , respectively, and $\sigma_{q', q}(E_0, Z)$ is the charge transfer cross-section from state q' to q . Since the multi-electron capture cross-section is much smaller than the single-electron capture cross-section, the change of charge states can be obtained by a stepwise change when $|q - q'| > 1$ [31]. Taking C^{2+} in this study as an example, when C^{2+} passes through target X, it requires three transformation steps to reach C^- :



ΔE_1 is the difference between the first ionization energy of C^{2+} and that of X; ΔE_2 is the difference between the first ionization energy of C^+ and that of X; ΔE_3 is the difference between the electron affinity of C and the first ionization energy of X. When $|\Delta E_3|$ is smaller, a higher charge-exchange probability can be realized [32]. Moreover, the first ionization energy of C is 11.26 eV and the electron affinity is 1.26 eV [31], so selecting a target with lower ionization energy is beneficial for achieving conversion of C^{2+} to C^- ions.

During the stepwise conversion, the single-electron capture cross-section is calculated by the integral in Eq. (5) [33]:

$$\sigma = 2\pi \int_0^\infty bP(b) db$$

where $P(b)$ denotes the probability function of collision-induced charge transfer with respect to the impact parameter b , and $bP(b)$ reflects the weighted contribution of different impact parameters to the total cross-section. In general, the charge transfer cross-section obtained based on Eq. (5) for incident ions with energies of 30–300 keV is on the order of 10^{-16} – 10^{-15} cm^2 , and the specific cross-section is closely related to parameters such as the energy range of the collision system and the mass of the target atom [33]. Variation of these parameters not only changes the value of the collision cross-section but also significantly affects the electron transition channel and the charge state distribution of the final product [34]. Therefore, to improve the charge exchange efficiency from C^{2+} to C^- ions, it is crucial to investigate the effects of target species, ion incident energy, and charge exchange cell structure on the electron capture process of C^{2+} .

III. PHYSICAL MODELING

The processes of particle-matter interaction in Geant4 are categorized under the electromagnetic interaction module and the strong interaction module [35–37]. Electromagnetic interactions include processes such as multiple scattering, ionization, photoelectric effect, and bremsstrahlung, while strong interactions include elastic scattering, inelastic scattering, and transmutation of atomic nuclei. The Geant4 physical model library used in this study is FTFP_{BERT} [35, 38], which accurately describes the elastic and inelastic scattering processes of low-energy particles in matter and can thus be used to simulate various physical processes occurring in charge exchange.

To verify the validity of this simulation model, the physical model for charge exchange with $C^{2+} \rightarrow C^-$ is constructed in Geant4 with reference to the parameters of the charge exchange cell adopted by Prof. Freeman and his team [25, 39] in PIMS experiments, as shown in Fig. 1 [Figure 1: see original paper]. The pressure distribution of the target in the charge exchange cell is shown in Fig. 2 [Figure 2: see original paper]. In Geant4 settings, equivalent areal density S is used instead of pressure (P); the transformation is detailed in references [40, 41].

[Figure 1: see original paper] shows that the simulation model comprises a charge exchange cell, parallel plate deflection electrodes, and a ΔE - E telescope detector system for ion detection. The charge exchange cell adopts a cylindrical structure (diameter of 20 mm, length adjustable up to 500 mm), in which the inside of the tube is filled with gas target material for charge exchange, enabling a high-pressure distribution in the middle and low-pressure distribution at both ends. Parallel plate deflector electrodes are installed at the exit of the charge exchange cell to achieve longitudinal spatial separation of ions with different energies and charge states by applying an electrostatic field perpendicular to the beam direction. The ΔE - E telescope detector system utilizes the segmented energy deposition of charged ions within the sensitive volume of the detector to achieve particle identification and statistics. The thickness parameters of the different detectors were obtained by calculating the range of C^{2+} ions in the energy range of 30–300 keV using SRIM software [42]; Si crystals with a thickness of 0.25 μm were selected for the ΔE detector and CsI crystals with a thickness of 300 μm were selected for the E detector.

According to Eq. (6), the deflection angle of charged ions in a deflection electric field was calculated and the detectors were placed on the deflection paths of C^0 , C_{\pm} , and C^{2-} ions. The longitudinal distance was adjusted to ensure that detectors at each angle would not block each other, thereby enabling effective recording of the number of ions in different charge states. In Eq. (6), U is the voltage between the two electrode plates, L is the length of the electric field, d is the spacing between the two electrode plates, m is the ion mass, and E is the ion energy.

$$\theta = \arctan\left(\frac{qeUL}{2mEd^2}\right)$$

Based on the established physical model, the C^-/C^+ yield ratio was computed and is depicted in Fig. 3 [Figure 3: see original paper]. The simulation results show good agreement with the experimental data reported by Prof. Freeman et al. [25] in the 60–250 keV energy region, with an average relative deviation of less than 0.3%, which verifies the reliability of the constructed simulation model. The significant deviation at 290 keV may result mainly from the approximate treatment of the gas density gradient distribution in the simulation, which cannot accurately reproduce the continuous distribution of gas density in the actual charge exchange cell; this simplified treatment leads to deviation in the yield of

C⁺ ions. These results demonstrate that the charge exchange cell model constructed using Geant4 can effectively simulate the ion charge exchange process across a wide energy range with good accuracy and applicability.

[Figure 3: see original paper] Comparison between simulation results and experimental validation [25]

IV. RESULTS AND DISCUSSION

Using the physical model built in Geant4, we adjusted the target density, charge exchange cell structure, and incident ion energy to explore their effects on charge exchange efficiency. To analyze the charge state distribution of incident ions more intuitively, we used the following equations to calculate the yield of each charge state:

$$P_{n\pm} = \frac{C_{n\pm}}{C_{2+}^{\text{in}}} \times 100\%$$

where $C_{\{n\pm\}}$ denotes the ion counts for a given charge state and $C_{\{2+\}}^{\text{in}}$ is the total count of incident C²⁺ ions. This equation enables calculation of the yield of ions in each charge state relative to the total number of incident C²⁺ ions, providing a uniform benchmark for comparing the distribution of each charge state under different simulation conditions.

A. Effect of Target Type and Density on Charge Exchange Efficiency

As previously described, charge exchange efficiency can be improved by selecting target gases with low ionization energy. In this study, 60 keV C²⁺ ions were used as the incident beam, and methane (ionization energy 12.61 eV [43]) and isobutane (ionization energy 10.57 eV [44]) were selected as targets to investigate the effect of different targets on charge exchange efficiency under gradient density distribution. The areal density of the target material with gradient density distribution is quantified using weighted areal density, calculated by summing the products of gradient-specific thicknesses multiplied by their length-weighted ratios.

The simulation results shown in Fig. 4 [Figure 4: see original paper] reveal that under identical charge exchange cell length and gradient density distribution, the number of C⁻ ions produced using isobutane as the target material is larger than that produced using methane, which is consistent with experimental results—likely because isobutane has higher electronegativity [25], making it a better electron donor and facilitating electron capture by C²⁺ to generate C⁻. By examining the relationship between the yields of ions with different charge states and the target material density (Fig. 5 Figure 5: see original paper), we observe that the number of C⁻ ions gradually increases with target density. When the target material reaches a certain density, the yield of C⁻ ions reaches a maximum. Beyond this point, further increases in target density lead to a

rise in the yield of C^{2-} ions. This behavior can be attributed to enhanced collisions between carbon ions and the medium as the areal density increases, giving initially formed C^- ions a greater chance to capture additional electrons and form C^{2-} ions. The evolution trends of C^-/C^{2+} and C^+/C^{2+} at different areal densities are shown in Fig. 5(b), which further demonstrates the gradual transformation process from C^{2+} to C^- ions passing through target media and is consistent with previous experimental results [27].

[Figure 4: see original paper] The C^- proportion of incident C^{2+} particles at 60 keV with different target gases, CH_4 and isobutane

B. Effect of Charge Exchange Cell Structure on Charge Exchange Efficiency

The structure of the charge exchange cell has a decisive impact on charge exchange efficiency. On one hand, to enhance efficiency, the cell must be sufficiently long to strengthen interactions between ions and target material. On the other hand, low-energy ions are more susceptible to scattering during collisions, and an excessively long cell may increase beam divergence, thereby degrading beam quality. In practical experiments, the structure of the charge exchange cell is not easily modified; however, in simulation models, it is possible to study the influence of cell structure on charge exchange efficiency by adjusting the cell geometry and the density distribution of the target material within it.

In this study, four types of charge exchange cell structures were investigated: (a) a 500 mm cell with equal-length density gradient distribution; (b) a 700 mm cell with low-density gradient left-biased toward the deflector side; (c) a 700 mm cell with low-density gradient right-biased toward the beam entrance; and (d) a 700 mm cell with symmetric low-density gradients on both ends. The simulation models are illustrated in Fig. 6 [Figure 6: see original paper] (left). The corresponding distributions of C^- ion yield ratios as a function of the weighted areal density of the target material under different structural configurations are shown in Fig. 6 (right). It is evident that when the length of the low-density region on the side closer to the deflection electrode is increased from 50 mm to 250 mm, the charge exchange efficiency improves significantly—by approximately 50%. In contrast, extending the length of the low-density region on the beam entrance side of the charge exchange cell does not lead to a notable change in efficiency. This may be attributed to the fact that when low-energy carbon ions collide with high-density target materials, their energy loss is greater than when colliding with low-density targets, resulting in a higher probability of carbon ions (atoms) capturing electrons. These results indicate that the presence of low-density regions can potentially enhance ion conversion efficiency and that the design of a charge exchange cell with an appropriate length is critical for optimal performance in positive-ion AMS systems.

[Figure 6: see original paper] Schematic diagrams of the charge exchange models (left) and C^- proportion of incident C^{2+} particles at 60 keV (right)

C. Effect of Incident Ion Energy on Charge State Distribution

The relationship between incident ion energy and charge exchange efficiency was further investigated in the simulation model. Specifically, we examined the relationship between incident energy ranging from 60 to 300 keV and the C^- yield after C^{2+} ions pass through charge exchange cells of identical structure but filled with different target gases (methane and isobutane).

Fig. 7 [Figure 7: see original paper] presents the variation of different ion yields with respect to incident ion energy during the charge exchange process. It can be observed that in both target gases, the yield of C^- ions exhibits a gradual decrease as incident ion energy increases, while the yield of neutral carbon atoms (C^0) rises sharply, resulting in a continuous reduction in the average charge state of the system. This trend may be attributed to the higher electron capture cross-section at lower energies [45] and the higher electron loss cross-section at higher energies [46]. Therefore, to achieve high charge exchange efficiency in positive-ion AMS using methane or isobutane as target gases, the incident energy of C^{2+} ions should be kept below 100 keV.

[Figure 7: see original paper] Charge-state distributions of carbon ions (60–300 keV) interacting with (a) methane and (b) isobutane

V. CONCLUSION

In this study, the Monte Carlo toolkit Geant4 was employed for the first time to simulate the charge exchange process from C^{2+} to C^- . By analyzing the yields of ions with different charge states, we investigated the effects of target gas species, incident ion energy, and target gas density distribution on charge exchange efficiency. The results indicate that under identical charge exchange cell structures and incident ion energies, different target gases yield varying conversion efficiencies from C^{2+} to C^- . Among non-metallic gases, isobutane exhibits higher charge exchange efficiency compared to methane. Notably, when methane is used as the target gas, the maximum conversion efficiency from C^{2+} to C^- can reach up to 2%. Furthermore, non-uniformity in gas density within the charge exchange cell has a pronounced impact on the distribution of ion charge states at the exit, with the presence of low-density regions showing a tendency to enhance conversion efficiency. These findings can provide important theoretical guidance for the design and optimization of positive-ion AMS systems.

REFERENCES

- [1] O. Langer, J. Song, M.S. Choi et al., Accelerator mass spectrometry for quantification of micro- and therapeutic-dose diclofenac in microdialysis samples. *Bioanalysis* **14**, 1111–1122 (2022). <https://doi.org/10.4155/bio-2022-0064>
- [2] S. Kim, J.H. Kwak, J.K. Jung et al., Method development for ^{14}C -labeling of IgG antibodies in preparation for clinical trials. *Journal of Analytical Science*

and Technology **15**, 6 (2024). <https://doi.org/10.1186/s40543-024-00420-w>

[3] G. Lappin, R.C. Garner, Big physics, small doses: the use of AMS and PET in human microdosing of development drugs. *Nature Reviews Drug Discovery* **2**, 233–240 (2003). <https://doi.org/10.1038/nrd1037>

[4] J. He, M. Liang, C. Anying, Degassing membrane for ^{14}C detection in water. *Journal of Tsinghua University (Science and Technology)* **60**, 341–347 (2020). <https://doi.org/10.16511/j.cnki.qhdxxb.2019.26.047>

[5] Y. Asscher, S. Weiner, E. Boaretto, A new method for extracting the insoluble occluded carbon in archaeological and modern phytoliths: Detection of ^{14}C -depleted carbon fraction and implications for radiocarbon dating. *Journal of Archaeological Science* **78**, 57–65 (2017). <https://doi.org/10.1016/j.jas.2016>

[6] W. Kutschera, Accelerator mass spectrometry: state of the art and perspectives. *Advances in Physics: X* **1**, 570–595 (2016). <https://doi.org/10.1080/23746149.2016.1224603>

[7] M.S. Oh, G.H. Lee, Y. Kim et al., Study on the pharmacokinetics and distribution of exogenous taurine in a brain by ^{14}C -nanotracing technique based on accelerator mass spectrometry. *Journal of Pharmaceutical and Biomedical Analysis* 116986 (2025). <https://doi.org/10.1016/j.jpba.2025.116986>

[8] C. Xie, D. Xu, Y. Han et al., AMS radiocarbon dating of K4 sacrificial pit at Sanxingdui site in Guanghan City, Sichuan Province. *Sichuan Cult Relics* **216**, 117–120 (2021).

[9] T. Doğan, E. İlkmen, F. Kulak, Radiocarbon analysis and status report from Türkiye: 1MV national AMS laboratory (TUBITAK-AMS). *Radiocarbon* **65**, 375–388 (2023). <https://doi.org/10.1017/RDC.2023.8>

[10] S.P. Freeman, G.T. Cook, A.B. Dougans et al., Improved SSAMS performance. *Nuclear Instruments and Methods in Physics Research Section B: Beam Interactions with Materials and Atoms* **268**, 715–717 (2010). <https://doi.org/10.1016/j.nimb.2009.10.012>

[11] M. He, Y. Pang, Y. Bao et al., Performance of Home-Made Single-Stage ^{14}C AMS System at CIAE. *Radiocarbon* **61**, 1511–1516 (2019). <https://doi.org/10.1017/RDC.2019.17>

[12] M. Hotchkis, T. Wei, Radiocarbon detection by ion charge exchange mass spectrometry. *Nuclear Instruments and Methods in Physics Research Section B: Beam Interactions with Materials and Atoms* **259**, 158–164 (2007). <https://doi.org/10.1016/j.nimb.2007.01.153>

[13] W. Kutschera, A.J.T. Jull, M. Paul et al., Atom counting with accelerator mass spectrometry. *Reviews of Modern Physics* **95**, 035006 (2023). <https://doi.org/10.1103/RevModPhys.95>

[14] B. Marcante, L. Marino, N.E. Cattaneo et al., Advancing forensic human chronological age estimation: Biochemical, genetic, and epigenetic approaches

from the last 15 years: A systematic review. *International Journal of Molecular Sciences* **26**, 3158 (2025). <https://doi.org/10.3390/ijms26073158>

[15] Y. Wang, X. Chen, A.D. Switzer et al., About 868 cal. yr BP tsunami event at the northern South China Sea revealed from off-shore sediments. *Global and Planetary Change* **245**, 104685 (2025). <https://doi.org/10.1016/j.gloplacha.2024.104685>

[16] B.Á. Baráth, T. Varga, I. Major et al., Investigating the impact of COVID-19 on the atmospheric ^{14}C trend and fossil carbon load at urban and background sites in Hungary. *Radiocarbon* **67**, 251–264 (2025). <https://doi.org/10.1017/RDC.2024.133>

[17] T. Schulze-König, M. Seiler, M. Suter et al., The dissociation of ^{13}CH and $^{12}\text{CH}_2$ molecules in He and N_2 at beam energies of 80–250 keV and possible implications for radiocarbon mass spectrometry. *Nuclear Instruments and Methods in Physics Research Section B: Beam Interactions with Materials and Atoms* **269**, 34–39 (2011). <https://doi.org/10.1016/j.nimb.2010.09.015>

[18] J. Park, W. Hong, G. Park et al., Development of a molecular removal method for minimizing interference in radiocarbon (^{14}C) measurements using laser technology. *Nuclear Instruments and Methods in Physics Research Section B: Beam Interactions with Materials and Atoms* **563**, 165714 (2025). <https://doi.org/10.1016/j.nimb.2025.165714>

[19] M. Roberts, R. Culp, D. Dvoracek et al., The ^{14}C AMS system at the University of Georgia. *Nuclear Instruments and Methods in Physics Research Section B: Beam Interactions with Materials and Atoms* **223**, 1–4 (2004). <https://doi.org/10.1016/j.nimb>

[20] H. Lee, A. Galindo-Uribarri, K. Chang et al., The $^{14}\text{CH}_2$ molecule and radiocarbon dating by accelerator mass spectrometry. *Nuclear Instruments and Methods in Physics Research Section B: Beam Interactions with Materials and Atoms* **5**, 208–210 (1984). [https://doi.org/10.1016/0168-583X\(84\)](https://doi.org/10.1016/0168-583X(84))

[21] H.A. Synal, S. Jacob, M. Suter, The PSI/ETH small radiocarbon dating system. *Nuclear Instruments and Methods in Physics Research Section B: Beam Interactions with Materials and Atoms* **172**, 1–7 (2000). [https://doi.org/10.1016/S0168-583X\(00\)00376-1](https://doi.org/10.1016/S0168-583X(00)00376-1)

[22] T. Goslar, J. Czernik, E. Goslar, Low-energy ^{14}C AMS in Poznań radiocarbon laboratory, Poland. *Nuclear Instruments and Methods in Physics Research Section B: Beam Interactions with Materials and Atoms* **223**, 5–11 (2004). <https://doi.org/10.1016/j.nimb.2004.04.005>

[23] J.B. Schroeder, T.M. Hauser, G.M. Klody et al., Initial results with low energy single stage AMS. *Radiocarbon* **46**, 1–4 (2004). <https://doi.org/10.1017/S003382220003928X>

[24] H.A. Synal, M. Döbeli, S. Jacob et al., Radiocarbon AMS towards its low-energy limits. *Nuclear Instruments and Methods in Physics Research Sec-*

- tion B: Beam Interactions with Materials and Atoms* **223**, 339–345 (2004). <https://doi.org/10.1016/j.nimb.2004.04.067>
- [25] S.P. Freeman, R.P. Shanks, X. Donzel et al., Radiocarbon positive-ion mass spectrometry. *Nuclear Instruments and Methods in Physics Research Section B: Beam Interactions with Materials and Atoms* **361**, 229–232 (2015). <https://doi.org/10.1016/j.nimb.2015.04.034>
- [26] K. Wilcken, S. Freeman, S. Xu et al., Attempted positive ion radiocarbon AMS. *Nuclear Instruments and Methods in Physics Research Section B: Beam Interactions with Materials and Atoms* **268**, 712–714 (2010). <https://doi.org/10.1016/j.nimb.2009.10.011>
- [27] K. Li, S. Peng, T.H. Ma et al., in *Journal of Physics: Conference Series*, Preliminary results of positive ion mass spectrometry based on a 2.45 GHz ECR ion source and a non-metallic gas target. Vol. 2244, IOP Publishing, 2022, p. 012093, <https://doi.org/10.1088/1742-6596/2244/1/012093>
- [28] R. Middleton, in *Proceedings of the First Conference on Radiocarbon Dating With Accelerators: Held at the University of Rochester, April 20 and 21, 1978*, On the Possibility of Counting ^{14}C -Ions. University of Rochester, 1978
- [29] W. Wu, S. Peng, T. Ma et al., A 2.45 GHz microwave ion source for carbon positive-ion mass spectrometry. *Journal of Instrumentation* **15**, P03028 (2020). <https://doi.org/10.1088/1748-0221/15/03/P03028>
- [30] Y.A. Belkova, N.V. Novikov, Y.A. Teplova, Influence of energy losses on charge distribution of fast ions passing through solid matter. *Modern Physics Letters B* **34**, 2050150 (2020). <https://doi.org/10.1142/S021798492050150X>
- [31] R. Hellborg, *Electrostatic Accelerators*, (Springer, 2005)
- [32] H.S.W. Massey, Collisions between atoms and molecules at ordinary temperatures. *Reports on Progress in Physics* **12**, 248 (1949). <https://doi.org/10.1088/0034-4885/12/1/311>
- [33] N. Stolterfoht, R. Cabrera-Trujillo, Y. Öhrn et al., Strong Isotope Effects on the Charge Transfer in Slow Collisions of He^{2+} with Atomic Hydrogen, Deuterium, and Tritium. *Physical Review Letters* **99**, 103201 (2007). <https://doi.org/10.1103/PhysRevLett.99.103201>
- [34] B. WEI, R. ZHANG, Highly charged atomic physics: Charge exchange and its application in X-ray astrophysical modeling. *Scientia Sinica Physica, Mechanica & Astronomica* **55**, 250008 (2025). <https://doi.org/10.1360/SSPMA-2024-0469>
- [35] S. Agostinelli, J. Allison, K. Amako et al., GEANT4—a simulation toolkit. *Nuclear Instruments and Methods in Physics Research Section A: Accelerators, Spectrometers, Detectors and Associated Equipment* **506**, 250–303 (2003). [https://doi.org/10.1016/S0168-9002\(03\)01368-8](https://doi.org/10.1016/S0168-9002(03)01368-8)

[36] T. Shi-Biao, Y. Ze-Jie, H. Huang et al., Geant4 used in medical physics and hadrontherapy technique. *Nuclear Science and Techniques* **17**, 276–279 (2006). [https://doi.org/10.1016/S1001-8042\(06\)60051-1](https://doi.org/10.1016/S1001-8042(06)60051-1)

[37] A. Lamrabet, A. Maghnoij, J. Tajmouati et al., Assessment of the power deposition on the MEGAPIE spallation target using the GEANT4 toolkit. *Nuclear Science and Techniques* **30**, 1–7 (2019). <https://doi.org/10.1007/s41365-019-0590-6>

[38] Geant4 Collaboration, *Geant4 User's Guide*, available from: <http://geant4.web.cern.ch/geant4/G4UsersDoc> (2024)

[39] R. Hellborg, M. Kiisk, P. Persson et al., Vacuum in an accelerator system—calculations and measurements. *Vacuum* **78**, 427–434 (2005). <https://doi.org/10.1016/j.vacuum.2005.01.063>

[40] D.R. Tilley, *Thermal Physics* (2nd edn). *Physics Bulletin* **31**, 321 (1980). <https://doi.org/10.1088/0031-9112/31/9/055>

[41] M. Nic, L. Hovorka, J. Jirat et al., *IUPAC Compendium of Chemical Terminology—the Gold Book*, (International Union of Pure and Applied Chemistry, 2005), <https://doi.org/10.1351/goldbook.S06167>

[42] J.F. Ziegler, M. Ziegler, J. Biersack, SRIM—the stopping and range of ions in matter (2010). *Nuclear Instruments and Methods in Physics Research Section B: Beam Interactions with Materials and Atoms* **268**, 1818–1823 (2010). <https://doi.org/10.1016/j.nimb.2010.02.091>

[43] J.F. Ziegler, M. Ziegler, J. Biersack, The ionization potentials of CH₄ and CD₄. *J. Chem. Phys* **86**, 674–676 (1987). <https://doi.org/10.1063/1.452268>

[44] Y.R. Luo, P.D. Pacey, Effects of alkyl substitution on ionization energies of alkanes and haloalkanes and on heats of formation of their molecular cations Part 2.* Alkanes and chloro-, bromo- and iodoalkanes. *International Journal of Mass Spectrometry and Ion Processes* **112**, 63–77 (1992). [https://doi.org/10.1016/0168-1176\(92\)87032-A](https://doi.org/10.1016/0168-1176(92)87032-A)

[45] L.M. Rottmann, R. Bruch, P. Neill et al., Single-electron capture by 100–1500 keV C⁺ ions in several atomic and molecular targets. *Physical Review A* **46**, 3883–3888 (1992). <https://doi.org/10.1103/PhysRevA.46.3883>

[46] M. Suter, S. Maxeiner, H.A. Synal et al., Charge-state distributions and charge-changing cross sections and their impact on the performance of AMS facilities. *Nuclear Instruments and Methods in Physics Research Section B: Beam Interactions with Materials and Atoms* **437**, 116–122 (2018). <https://doi.org/10.1016/j.nimb.2018.08.014>

Note: Figure translations are in progress. See original paper for figures.

Source: ChinaXiv — Machine translation. Verify with original.